Modification of Electrical Properties of Graphene by Substrate-Induced Nanomodulation

ARTICLE *in* NANO LETTERS · JULY 2013

Impact Factor: 13.59 · DOI: 10.1021/nl400827p · Source: PubMed

NANO LETTERS

Letter

pubs.acs.org/NanoLett

Modification of Electrical Properties of Graphene by Substrate-Induced Nanomodulation

Jong-Kwon Lee,[†] Shiro Yamazaki,[‡] Hoyeol Yun,[§] Jinwoo Park,[∥] Gary P. Kennedy,[†] Gyu-Tae Kim,[†] Oswald Pietzsch,[‡] Roland Wiesendanger,[‡] SangWook Lee,[§] Suklyun Hong,*[,∥] Urszula Dettlaff-Weglikowska,*[,†] and Siegmar Roth[†]

[†]School of Electrical Engineering, WCU on Flexible Nanosystems, Korea University, Seoul 136-713, Korea

[‡]Institute of Applied Physics and INCH, University of Hamburg, 20355 Hamburg, Germany

[§]Division of Quantum Phases and Device, School of Physics, Konkuk University, Seoul 143-701, Korea

[∥]Department of Physics and Graphene Research Institute, Sejong University, Seoul 143-747, Korea

Supporting Information

ABSTRACT: A periodically modulated graphene (PMG) generated by nanopatterned surfaces is reported to profoundly modify the intrinsic electronic properties of graphene. The temperature dependence of the sheet resistivity and gate response measurements clearly show a semiconductor-like behavior. Raman spectroscopy reveals significant shifts of the G and the 2D modes induced by the interaction with the underlying grid-like nanostructure. The influence of the periodic, alternating contact with the substrate surface was studied in terms of strain caused by bending of graphene and doping through chemical interactions with underlying substrate atoms. Electronic structure calculations performed on a model of PMG reveals that it is possible to tune a band gap within 0.14−0.19 eV by considering both the periodic mechanical bending and the surface coordination chemistry. Therefore, the PMG can be regarded as a further step toward band gap engineering of graphene devices.

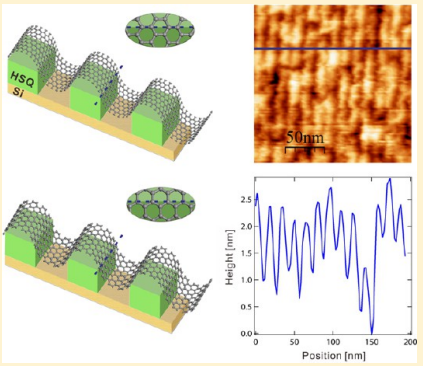

KEYWORDS: *Graphene, bandgap, periodic nanomodulation, superstructure*

Graphene is a promising candidate for future high-speed electronics.[1−5] However, its practical use is inhibited because it has a zero band gap.[6,7] Efforts to modify the electronic band structure have focused on constraining graphene in nanoribbons, nanomesh structures, applying an electric field across graphene bilayers, chemical functionalization, and the application of uniaxial strain.[8−13] However, nonuniform nanoribbon edge geometry,[14] high electric fields across bilayers,[15] reduced conductivity of chemically functionalized graphene,[16] and large strains of >20%[17] prevent the effective use of graphene in devices. In addition to the electronic properties, the high elasticity and mechanical robustness of graphene suggests that it has excellent potential for controllable physical deformation involving large-angle bending.[18−20] Following a theoretical study on the anisotropic behavior of graphene in a periodic potential,[21] investigations on controlled ripple texturing of suspended graphene and tuning a band gap using electrostatic gates in strained graphene were reported.[22,23] As a monatomic thin layer, graphene can conform mechanically to any nanostructured surface.

In this Letter, we explore a new concept of band gap engineering of graphene by investigating the effect of a periodic, partially suspended graphene, which has an alternating contact with the substrate. Such a periodically modulated graphene (PMG) was achieved by the graphene suspension onto an array of nanotrenches patterned into the substrate. The conformability of graphene found in PMG implies strong chemical interaction with the substrate. The periodically changed coordination chemistry involved in the repeatable partial contacts of graphene with the underlying substrate may open a band gap. Furthermore, a periodically induced strain along the nanotrenches is thought to contribute to the modification of the electronic band structure of graphene.

To prove the substrate induced modulation in graphene several samples were prepared (Supplementary Figure S1). For testing the mechanical and electrical behavior of graphene placed on a nanopatterned surface, a periodic quasi one-dimensional line pattern with 10 nm line width was fabricated by e-beam lithography in a hydrogen silesquioxane (HSQ) layer. Nanotrenches with dimensions (10 × 10) nm with a 10 nm spacing were formed, as shown schematically in Figure 1a. Then, a single graphene sheet, mechanically cleaved on a SiO_2/Si wafer, was transferred on top of the nanostructure using poly(methyl methacrylate) (PMMA). The resulting stretch−strain was detected by Raman measurements. A scanning electron microscope (SEM) image (Figure 1b) shows the

Received: March 6, 2013
Revised: July 5, 2013

   dx.doi.org/10.1021/nl400827p | *Nano Lett.* XXXX, XXX, XXX−XXX

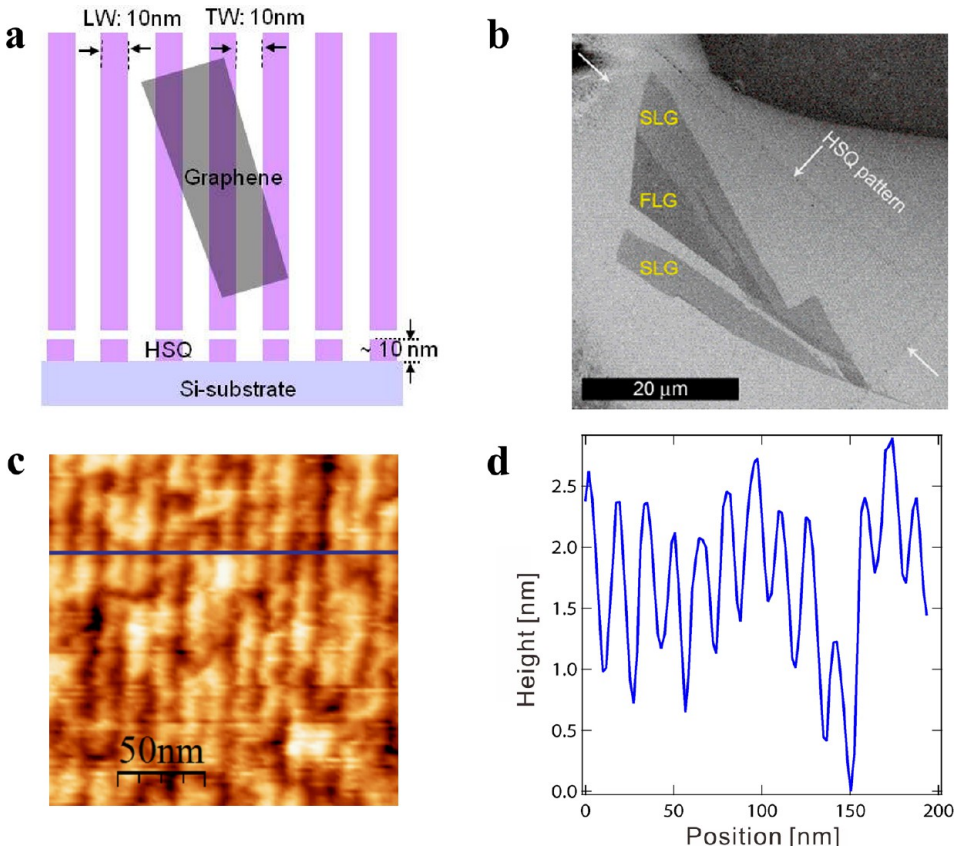

Figure 1. (a) Schematic illustration (not to scale) of the PMG attached to the periodic grid-like nanostructured substrate consisting of a 10 nm thick HSQ on Si with 10 nm line width (LW) and 10 nm trench width (TW). (b) SEM image showing single layers of graphene (SLG) and a few-layer graphene flake (FLG) located on a square (50 μm × 50 μm) of the HSQ pattern denoted by white arrows. (c) The surface morphology of PMG examined by STM and (d) a line section measured along the blue line showing the trench width of ~10 nm and an apparent depth of 1−2 nm.

location of graphene on the supporting nanostructure. The scanning tunneling micrograph (STM) presented in Figure 1c clearly demonstrates the graphene undulation as a function of the underlying nanotrenches. It reveals that the suspended graphene sheet is pulled down into each trench. The apparent undulation of 1−2 nm shown in the line profile (Figure 1d) may be a lower depth limit, since the tunneling tip, which is of finite width, is unable to probe the depth of the trenches accurately. Bright spots appearing on the STM image are PMMA residues.

To evaluate how the graphene undulation affects its vibrational modes, we measured the Raman spectra of several PMG samples and compared them with the spectra of a flat graphene (FG) reference sample placed on the same substrate. Significant red-shifts of both G mode (5.2−7.1 cm^{-1}) and 2D mode (8.3−12.2 cm^{-1}) were observed for random orientations of graphene with respect to the underlying nanotrenches (Supplementary Figure S2). Figure 2a shows the Raman spectrum of a PMG sample examined by STM; the 2D line is shifted by 9 cm^{-1} and the G by 5 cm^{-1}. These red-shifts indicate that the π electron system of PMG is affected by the underlying nanotrenches. While oxygen doping from the substrate corresponds to a blue-shift of the Raman peaks,[24,25] the stretching strain generates a red-shift. Since all of our PMG samples show a red-shift, strain must dominate. Compared with Mohiuddin et al. on Raman scattering in graphene under uniaxial strain,[26] we estimate that the red-shifts observed in our case correspond to an effective stretching strain of about 0.5%. If we include the charge doping from the interaction with O atoms which causes opposite changes in the Raman spectrum, then a tensile strain much higher than 0.5% is expected in PMG.

The existence of anisotropic strain in PMG was confirmed by the polarization-dependent Raman spectra. Figure 2b demonstrates schematically the orientation of the incident light polarization with respect to the strain direction (perpendicular to the trenches). The evolution of the G and 2D modes of PMG recorded for angles varying between 0° and 180° is shown in Figure 2c. Since the estimated strain in PMG is <1%, only a broadening of the G band indicates partially developed splitting into two components, G^- and G^+.[26] Nevertheless, the polarization-dependent intensities of the G^- and G^+ bands cause the position of the G band to shift within ~6 cm^{-1} as demonstrated in Figure 2d. The periodic shift of the 2D mode (Figure 2e) as a result of the sample orientation with respect to the polarized light also confirms the anisotropic nature of PMG and the strain orientation perpendicular to the nanotrenches. As PMG consists of a defined array of suspended parts with an alternating contact to the substrate, a periodically localized doping is also expected to cause interference of the two-dimensional electronic waves propagating, in particular, in the perpendicular direction to each trench and thus modifying the electrical transport in graphene.

We investigated the electrical transport properties of the PMG using STM tips as electrodes contacting the sample to perform four-point probe resistivity measurements as shown schematically in Figure 3a. In the SEM micrograph of Figure 3b the four probes can be seen in contact with the sample, in a

dx.doi.org/10.1021/nl400827p | Nano Lett. XXXX, XXX, XXX−XXX

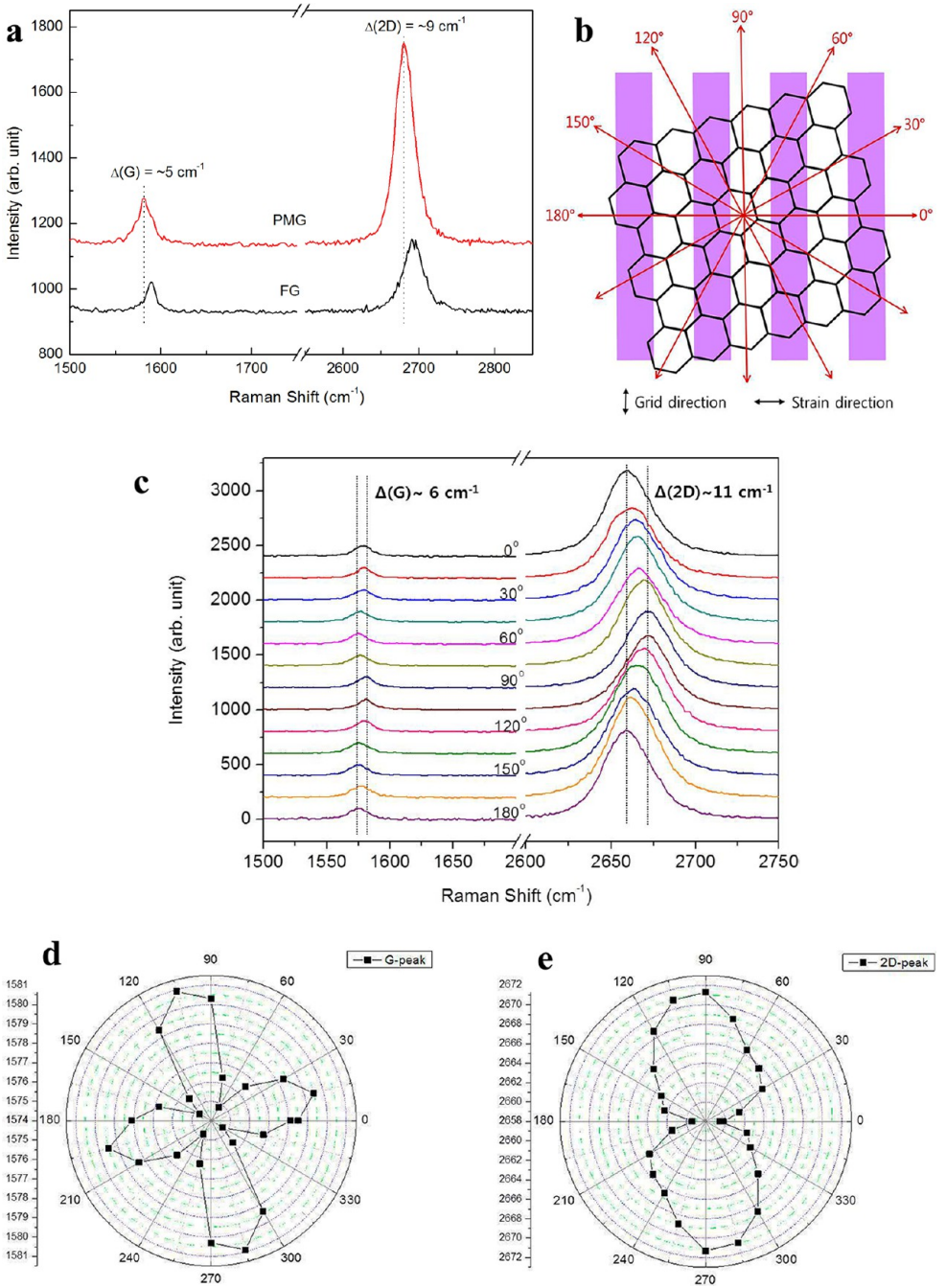

Figure 2. (a) Raman spectrum of the PMG in comparison with that of a flat graphene (FG) used as a reference sample. The dotted lines denote the positions of the G and 2D bands in PMG with respect to those in FG and demonstrate corresponding red-shifts. (b) Schematic (not to scale) illustrates the directions of the incident light polarization with respect to the PMG sample. The black arrows indicate the strain direction perpendicular to the grid trenches. (c) The evolution of the G- and 2D-bands of PMG as a function of the incident laser polarization relative to the strain direction. The dotted lines denote the extremal positions of the G and 2D bands when the polarization angle increases from 0° to 180°. (d,e) Polar plots of the G- and 2D-bands of PMG as a function of polarization angle, respectively.

typical arrangement along a line as carried out on various graphene sheets (flat and modulated). To exclude possible leakage current paths to the substrate during measurement, the dependence of the resistance on the distance between the voltage probes was proved for all room-temperature and low-temperature resistance measurements (Supplementary Figure S3). The measured sheet resistivity of 3−4 kΩ/sq is lower than the maximum sheet resistivity of $h/4e^2$ = 6.45 kΩ/sq for undoped graphene and reveals stronger charge doping than already known from graphene placed on SiO_2 (4−5 kΩ/sq).[6]

The behavior of the graphene resistivity upon cooling is an important indicator allowing us to distinguish between metallic and semiconducting properties. We measured the resistivity of PMG down to a temperature of 30 K. The sheet resistivity as a function of temperature T in the range from 30 to 300 K is plotted in Figure 3c. Typically, the resistivity of pristine graphene at the charge neutrality point decreases slightly upon cooling or stays constant.[27−29] However, we observe an increasing sheet resistivity by 2 orders of magnitude from 3 to 200 kΩ/sq as the temperature decreases toward 100 K.

dx.doi.org/10.1021/nl400827p | Nano Lett. XXXX, XXX, XXX−XXX

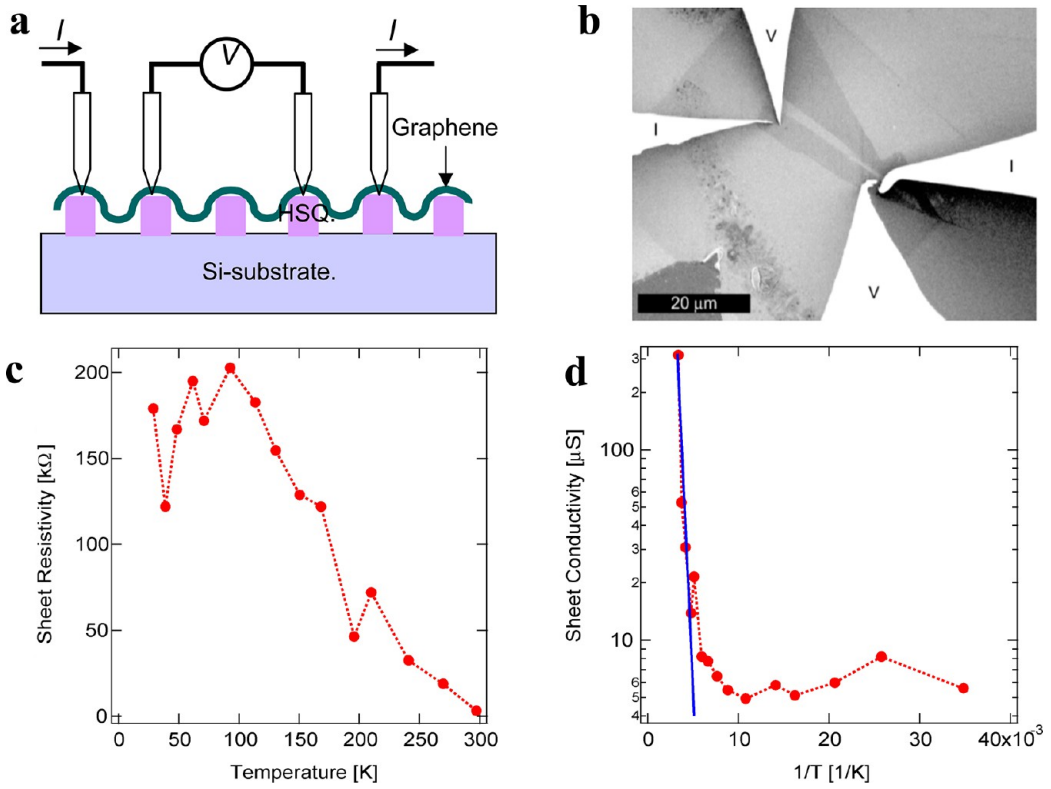

Figure 3. Electrical characterization of PMG over a grid-like nanostructure. (a) Schematic representation and (b) SEM image showing the arrangement of STM tips contacting the sample to perform four-probe resistivity measurements. (c) Temperature dependence of the sheet resistivity in PMG demonstrating semiconductor-like behavior. (d) Arrhenius plot used to determine the activation energy of PMG in the high temperature regime ($\sigma(T) = \sigma_o \exp(-\Delta E/k_B T)$, where ΔE is the activation energy related to the band gap and k_B is the Boltzmann constant).

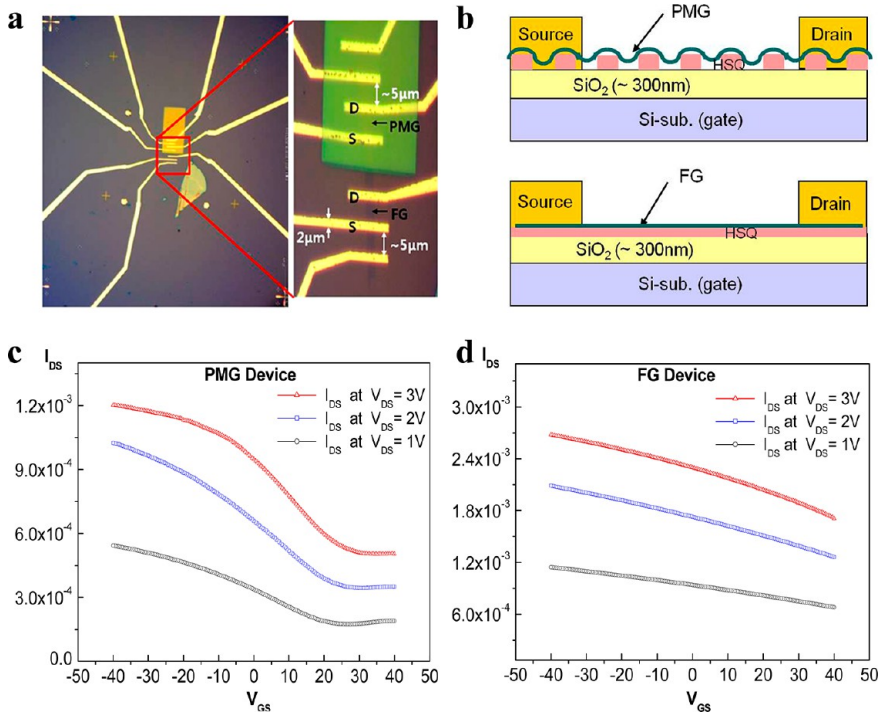

Figure 4. Transfer characteristics of the PMG and FG devices. (a) Optical microscopic images of the device structures fabricated on the same Si-substrate as a gate electrode, where the rectangular pattern represents the part modulated by HSQ line grids. The channel width/length defined by the source (S) and drain (D) electrodes is ~4 μm/5 μm. (b) Schematic side view of the PMG and FG devices. (c, d). Drain current (I_{DS}) versus gate voltage (V_{GS}) characteristics at constant drain−source voltages (V_{DS}) of 1, 2, and 3 V for the PMG and FG devices. The PMG device shows on/off characteristics with the Dirac point around $V_{GS} \sim 24$ V. The FG device demonstrates metallic properties at room temperature.

dx.doi.org/10.1021/nl400827p | Nano Lett. XXXX, XXX, XXX−XXX

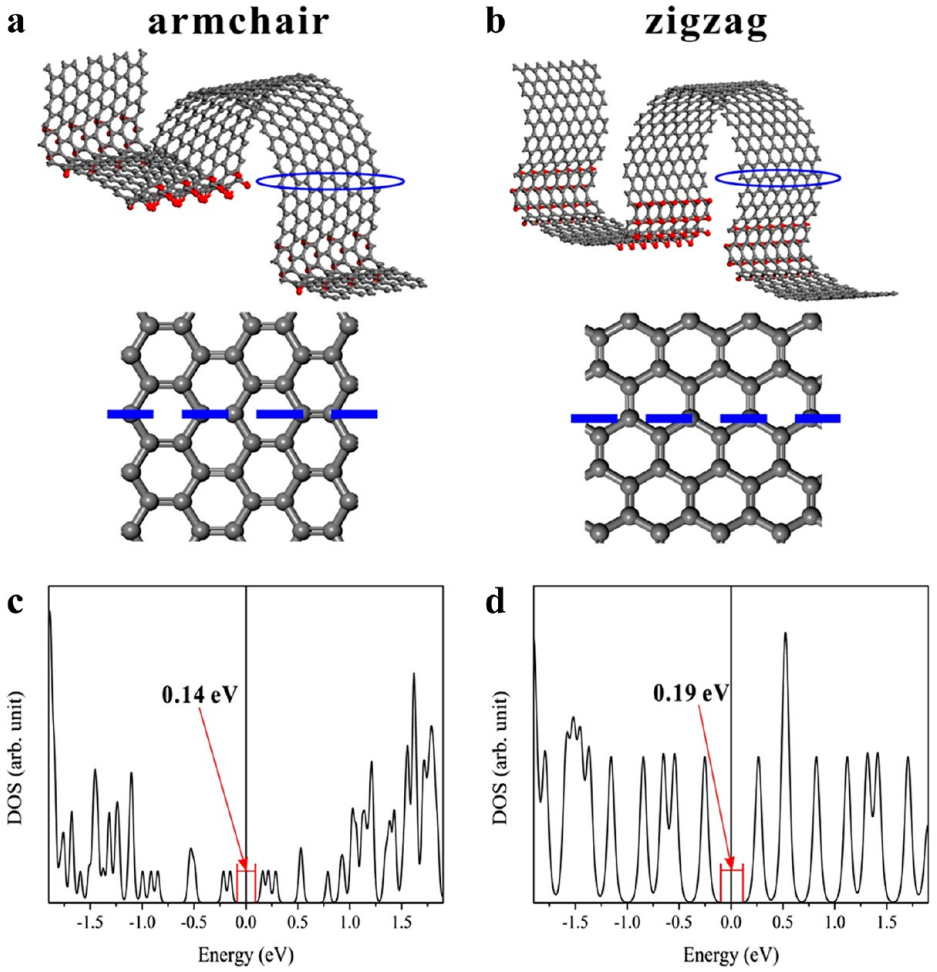

Figure 5. Periodic modulation of graphene supported by HSQ or SiO_2 substrate and related band structures. (a, b) Model structures of graphene mechanically modulated by bending and surface coordination chemistry stripes with a period of 4.4 nm. The blue lines show the modulation direction of the graphene lattices parallel to the armchair and the zigzag axes, respectively. The gray balls represent carbon, the red ones oxygen atoms. (c) Density of states (DOS) determined from the first-principles calculations based on DFT for graphene bent along the armchair axis demonstrating a band gap opening. (d) DOS for bending along the zigzag axis showing also a band gap opening.

Hence, PMG appears to have semiconductor-like behavior. The activation energy from the Arrhenius plot (Figure 3d) is ~0.2 eV. The general behavior of our data is consistent with the gap opening mechanism by an electrostatic potential in strained graphene as discussed by Row et al.,[23] where the pseudomagnetic fields created by the long-wavelength deformations are appropriately coupled with the electrostatic potential. The strain geometry in PMG is defined by the period of the underlying one-dimensional grid structure. The alternating potentials are generated in PMG by oxygen doping along the contact points to the substrate and spaced at a distance close to a half of the period of varying strains. Thus, the requirement for gap opening via strain with a commensurate electrostatic potential is fulfilled in the PMG structure. Concerning conductivity in the low temperature regime, further investigations are required to clarify whether variable range hopping or another conduction mechanism is responsible for the observed temperature dependence.

We also investigated the gate response of PMG and FG by fabricating device structures with an arrangement of electrodes in a transistor configuration on the periodically modulated and flat graphene areas (Figure 4a,b). Since a 10 nm layer of HSQ is insufficient to test the gate response, a 300 nm thermally grown SiO_2 layer on a Si substrate was used. Due to the postetching process connected with the fabrication of electrodes the nanotrench structure was enlarged to produce nanotrenches with a width of 20 nm and a 20 nm separation between trenches. A graphene sheet was transferred in such a way that it covered the nanostructured SiO_2 area as well as neighboring flat SiO_2 areas. The gate response of the resulting devices is presented in Figure 4c,d. Even with random orientation of the transferred graphene sheet with respect to the nanotrenches, the PMG device shows typical semiconducting properties, revealing an on/off ratio of about 3 and a mobility of 700−1000 $cm^2/(V\ s)$ at room temperature, while the FG device shows metallic property with a decrease in drain current as the gate voltage increases. The activation energy of 0.2 eV determined from the temperature dependence of PMG resistivity using STM tips as electric contacts is, however, not reflected in the performance of the PMG transistor. The reason for that is the current measurement in the transistor device can be affected by the postprocessing treatments (etching and lift-off process to deposit source/drain electrodes). Also, the profile of nanopattern and the orientation of graphene with respect to the strain direction are different in the two experiments. Furthermore, the FET device parameters (the gate insulator, the transistor channel width/length, and the contact electrodes) are still not optimized. Thus, the gate response at this state of

dx.doi.org/10.1021/nl400827p | *Nano Lett.* XXXX, XXX, XXX−XXX

research is definitely not competitive but can be improved by optimizing the device geometry and processing conditions.

To support our experimental results, we performed density functional theory (DFT) calculations on a graphene sheet which was suspended on the periodic nanostructure and is believed to partially interact with oxygen atoms from the supporting substrate. The graphene layer attached to the underlying nanostructure (Figure 5a,b) can be modeled by fully relaxed graphene strips. Chemical interaction of graphene with the SiO_2 surface, such as that found in HSQ,[30−32] is simulated by the adsorption of oxygen atoms on the bridge sites of graphene. These adsorbed oxygen atoms, increasing the concentration of positive charges, generate the partial and periodic charge doping in the modulated graphene. Bending of the graphene sheet was induced by the dimensions of the underlying nanotrenches, which are (2.2 × 2.2) nm with a separation distance of 2.2 nm. We scaled down the modulation period to 1:5 by comparison with the fabricated nanotrenches (10 × 10 × 10) nm to reduce the size of the calculated structure, while maintaining realistic trench dimensions. To investigate the effect of the modulation direction on the band gap of graphene, we considered the effect of bending along two special directions in which the bending lines of the graphene lattice are directed along the armchair and zigzag axes. Hence, we calculated the density of states (DOS) for these graphene deformations.

The calculated DOS for periodically deformed graphene are plotted as a function of energy in Figure 5c,d. A band gap opening of about 0.14 eV is calculated, when the graphene lattice is subject to bending along the armchair axis and the oxygen atoms from HSQ are periodically adsorbed. Likewise, a band gap of 0.19 eV is observed at the Fermi level as a result of a partial oxygen adsorption and modulation along the zigzag axis. Explanation of such behavior can be derived from the periodic bending and partial doping producing a graphene superlattice and mini bands due to a corresponding larger lattice constant and a smaller Brillouin zone. Calculations based on the induced curvature of the graphene lattice as a result of adhesion to the underlying nanotrenches show that the strain is modulated and varies periodically from −0.9% to 6.4% as the graphene sheet follows the curvature. Hence, lines of a periodic stretching and compressive strain are expected in PMG model along the modulation direction. Taking into account the average elongation of the graphene lattice parameters, an average stretching strain of 1.1% and 1.4% (orthogonal to the modulation direction) is calculated for the PMG geometries shown in Figure 5a,b, respectively (Supplementary Figure S4).

We also carried out DFT calculations for the cases in which there are periodic chemical doping without periodic corrugation and periodic corrugation without periodic doping to find out whether the surface coordination chemistry (or the corrugation) alone could open a band gap. The calculated DOS for two representative graphene lattice (armchair and zigzag) orientations parallel to the direction of nanotrenches are plotted as a function of energy in Supplementary Figures S5 and S6. Periodic oxygen doping produces a band gap only for the armchair orientation, while the periodic corrugation opens a band gap only for the zigzag orientation suggesting that a combination of periodic corrugation and chemical doping is needed for band gap opening.

In summary, the experimental results supported by the theoretical predictions provide a proof of principle that PMG can be regarded as a further step toward band gap engineering of graphene devices. We have shown that periodically nanomodulated graphene has the potential to modify the band structure of graphene through alternating contacts with a nanostructured substrate which changes the electrical properties from semimetallic to semiconducting. Since the nature of the modification depends upon the geometry of the underlying nanostructure, it should be possible to engineer semiconducting devices from graphene with diverse electrical properties. This means that PMG allows the fabrication of graphene devices with various band gaps by using nanostructured substrates with various geometries, which can easily be scaled for integrated circuits. This could be achieved by using largely conventional top-down mass-production techniques. As shown in our study, semimetallic properties of an unstrained graphene on flat substrate areas could be used as interconnects between devices, thus enabling the fabrication of all-carbon integrated circuits, with active devices placed in substrate locations having a nanotrench structure.

Methods. *Graphene Transfer Process.* The graphene sample was prepared by mechanically cleaving a graphite monocrystal on a 300 nm SiO_2/Si substrate. PMMA was spin-coated to a thickness of 500 nm on top of the exfoliated graphene sample. To detach the PMMA-graphene membrane the underlying SiO_2 layer was etched with 1 M KOH solution. Then, the graphene/PMMA film was transferred onto the predefined nanostructured substrate. Subsequently, the PMMA was removed by dipping in acetone at 50 °C for 1 h.

Raman Measurement. We studied the Raman spectra of graphene samples using micro-Raman spectroscopy. In this instrument, a monochromatic Ar-ion laser with a wavelength of 514.5 nm was used as the excitation source with a power of less than 1 mW to prevent sample heating.

STM and Transport Measurements. STM and transport measurements were carried out using a UHV-based variable-temperature four-probe STM equipped with a high-resolution SEM (UHV Nanoprobe, Omicron Nanotechnology). The positions of four STM tips in relation to the PMG were controlled with the aid of SEM images. STM imaging was performed by carefully moving the probe tip toward PMG using a high-resolution scanner, and then the STM function was used for imaging. Transport measurements were obtained by contacting the PMG with four STM tips. Current−voltage curves were recorded using a four-terminal measurement with a current source (Keithley model 6221) and a nanovoltmeter (Keithley model 2182A). The resistance of the graphene samples was determined from the slopes of current−voltage curves. This resistance was found to have linear probe-space dependence without an offset at the origin.

Fabrication of Field Effect Transistors. We fabricated bottom-gate type field-effect transistors with a channel width of ∼4 μm and a channel length of ∼5 μm. First, we made HSQ grid patterns with the line and trench widths of ∼20 nm on a 300 nm thick SiO_2 layer on Si-substrate. Then, PMG and FG were fabricated by transferring one graphene flake covering the grid and adjacent flat substrate area. Finally, the source and drain electrodes with 2 μm line width were patterned directly on top of the PMG and FG regions by applying e-beam lithography and depositing Au (35 nm)/Pd (10 nm) followed by a lift-off process.

DFT Calculations. We have performed DFT calculations within the generalized gradient approximation (GGA) using the Vienna ab initio simulation package (VASP). Plane waves up to an energy of 400 eV were included to expand the wave

dx.doi.org/10.1021/nl400827p | Nano Lett. XXXX, XXX, XXX−XXX

functions; the ions were represented by the projector augmented wave (PAW) potentials,[33,34] and van der Waals interactions[35] were used in Grimme's theory as implemented in VASP. All coordinates are fully relaxed until the Hellmann−Feynman forces are lower than 0.025 eV/Å. Periodically modulated graphene consists of a series of nanoscale smooth trenches deformed by the partial charge doping. The geometry of the PMG depends on the modulation direction with respect to the graphene lattice. Two cases are considered, where the bending lines of the graphene lattice being in contact with trench edges are directed along the armchair and the zigzag axes, respectively.

■ ASSOCIATED CONTENT

Supporting Information

Additional information on fabricated PMG samples and their Raman characteristics, sheet resistance measurement on the modulated graphene, strain calculation for the PMG geometries (Figure 5a,b), and DFT calculations supporting the concept of graphene corrugation combined with a periodic doping in PMG. This material is available free of charge via the Internet at http://pubs.acs.org.

■ AUTHOR INFORMATION

Corresponding Author

*E-mail: udettlaff.w@gmail.com; hong@sejong.ac.kr.

Notes

The authors declare no competing financial interest.

■ ACKNOWLEDGMENTS

This research was supported by the World Class University Projects (WCU) (R32-2008-000-10082-0, R31-2008-000-10057-0) through the National Research Foundation of Korea (NRF) funded by the Ministry of Education (MOE), and Nano Material Technology Development Program (2012M3A7B4049888), the Converging Research Center Program (2012K001310), and Basic Science Research Program (2012R1A2A2A01045496) through NRF funded by the Ministry of Science, ICT and Future Planning (MSIP), and Priority Research Centers Program (2010-0020207) through NRF/MOE. Furthermore, we would also like to thank the Hamburg Cluster of Excellence NANOSPINTRONICS, the Interdisciplinary Nanoscience Center Hamburg, and support from the DFG grant WI1277/25.

■ REFERENCES

(1) Novoselov, K. S.; Geim, A. K.; Morozov, S. V.; Jiang, D.; Zhang, Y.; Dubonos, S. V.; Grigorieva, I. V.; Firsov, A. A. *Science* **2004**, *306*, 666−669.
(2) Schwierz, F. *Nat. Nanotechnol.* **2010**, *5*, 487−496.
(3) Liao, L.; Bai, J.; Cheng, R.; Zhou, H.; Liu, L.; Liu, Y.; Huang, Y.; Duan, X. *Nano Lett.* **2012**, *12*, 2653−2657.
(4) Lin, Y.-M.; Valdes-Garcia, A.; Han, S.- J.; Farmer, D. B.; Meric, I.; Sun, Y.; Wu, Y.; Dimitrakopoulos, C.; Grill, A.; Avouris, P.; Jenkins, K. A. *Science* **2011**, *332*, 1294−1297.
(5) Wang, S.; Ang, P. K.; Wang, Z.; Tang, A. L.; Thong, J. T. L.; Loh, K. P. *Nano Lett.* **2010**, *10*, 92−98.
(6) Novoselov, K. S.; Geim, A. K.; Morozov, S. V.; Jiang, D.; Katsnelson, M. I.; Grigorieva, I. V.; Dubonos, S. V.; Firsov, A. A. *Nature* **2005**, *438*, 197−200.
(7) Geim, A. K. *Science* **2009**, *324*, 1530−1534.
(8) Han, M. Y.; Özyilmaz, B.; Zhang, Y.; Kim, P. *Phys. Rev. Lett.* **2007**, *98*, 206805.
(9) Bai, J.; Zhong, X.; Jiang, S.; Huang, Y.; Duan, X. *Nat. Nanotechnol.* **2010**, *5*, 190−194.
(10) Zhang, Y.; Tang, T.-T.; Girit, C.; Hao, Z.; Martin, M. C.; Zettle, A.; Crommie, M. F.; Shen, Y. R.; Wang, F. *Nature* **2009**, *459*, 820−823.
(11) Ohta, T.; Bostwick, A.; Seyller, T.; Horn, K.; Rotenberg, E. *Science* **2006**, *313*, 951−954.
(12) Luo, Z.; Vora, P. M.; Mele, E. J.; Charlie Johnson, A. T.; Kikkawa, J. M. *Appl. Phys. Lett.* **2009**, *94*, 111909.
(13) Ni, Z. H.; Yu, T.; Lu, Y. H.; Wang, Y. Y.; Feng, Y. P.; Shen, Z. X. *ACS Nano* **2008**, *2*, 2301−2305.
(14) Evaldsson, M.; Zozoulenko, I. V.; Xu, H.; Heinzel, T. *Phys. Rev. B* **2008**, *78*, 161407.
(15) Castro, E. V.; Novoselov, K. S.; Morozov, S. V.; Reres, N. M. R.; Lopes dos Santos, J. M. B.; Nilsson, J.; Guinea, F.; Geim, A. K.; Castro Neto, A. H. *Phys. Rev. Lett.* **2007**, *99*, 216802.
(16) Schniepp, H. C.; Li, J.-L.; McAllister, M. J.; Sai, H.; Herrera-Alonso, M.; Adamson, D. H.; Prud'homme, R. K.; Car, R.; Saville, D. A.; Aksay, I. A. *J. Phys. Chem. B* **2006**, *110*, 8535−8539.
(17) Pereira, V. M.; Castro Neto, A. H.; Peres, N. M. R. *Phys. Rev. B* **2009**, *80*, 045401.
(18) Briggs, B. D.; Nagabhirava, B.; Rao, G.; Geer, R.; Gao, H.; Xu, Y.; Yu, B. *Appl. Phys. Lett.* **2010**, *97*, 223102.
(19) Schniepp, H. C.; Kudin, K. N.; Li, J.-L.; Prud'homme, R. K.; Car, R.; Saville, D. A.; Aksay, I. A. *ACS Nano* **2008**, *2*, 2577−2584.
(20) Bao, W.; Myhro, K.; Zhao, Z.; Chen, Z.; Jang, W.; Jing, L.; Miao, F.; Zhang, H.; Dames, C.; Lau, C. N. *Nano Lett.* **2012**, *12*, 5470−5474.
(21) Park, C.-H.; Yang, L.; Son, Y.-W.; Cohen, M. L.; Louie, S. G. *Nat. Phys.* **2008**, *4*, 213−217.
(22) Bao, W.; Miao, F.; Chen, Z.; Zhang, H.; Jang, W.; Dames, C.; Lau, C. N. *Nat. Nanotechnol.* **2009**, *4*, 562−566.
(23) Low, T.; Guinea, F.; Katsnelson, M. I. *Phys. Rev. B* **2011**, *83*, 195436.
(24) Stampfer, C.; Molitor, F.; Graf, D.; Ensslin, K.; Jungen, A.; Hierold, C.; Wirtz, L. *Appl. Phys. Lett.* **2007**, *91*, 241907.
(25) Das, A.; Pisana, S.; Chakraborty, B.; Piscanec, S.; Saha, S. K.; Waghmare, U. V.; Novoselov, K. S.; Krishnamurthy, H. R.; Geim, A. K.; Ferrari, A. C.; Sood, A. K. *Nat. Nanotechnol.* **2008**, *3*, 210−215.
(26) Mohiuddin, T. M. G.; Lombardo, A.; Nair, R. R.; Bonetti, A.; Savini, G.; Jalil, R.; Bonini, N.; Basko, D. M.; Galiotis, C.; Marzari, N.; Novoselov, K. S.; Geim, A. K.; Ferrari, A. C. *Phys. Rev. B* **2009**, *79*, 205433.
(27) Chen, J.-H.; Jang, C.; Xiao, S.; Ishigami, M.; Fuhrer, M. S. *Nat. Nanotechnol.* **2008**, *3*, 206−209.
(28) Morozov, S. V.; Novoselov, K. S.; Katsnelson, M. I.; Schedin, F.; Elias, D. C.; Jaszczak, J. A.; Geim, A. K. *Phys. Rev. Lett.* **2008**, *100*, 016602.
(29) Tan, Y.-W.; Zhang, Y.; Stormer, H. L.; Kim, P. *Eur. Phys. J.* **2007**, *148*, 15−18.
(30) Shemella, P.; Nayak, S. K. *Appl. Phys. Lett.* **2009**, *94*, 032101.
(31) Kang, Y.-J.; Kang, J.; Chang, K. J. *Phys. Rev. B* **2008**, *78*, 115404.
(32) Ishigami, M.; Chen, J. H.; Cullen, W. G.; Fuhrer, M. S.; Williams, E. D. *Nano Lett.* **2007**, *7*, 1643−1648.
(33) Blöchl, P. E. *Phys. Rev. B* **1994**, *50*, 17953−17979.
(34) Kresse, G.; Joubert, D. *Phys. Rev. B* **1999**, *59*, 1758−1775.
(35) Grimme, S. *J. Comput. Chem.* **2006**, *27*, 1787−1799.

■ NOTE ADDED AFTER ASAP PUBLICATION

This Letter was published ASAP on July 19, 2013. One sentence in the "DFT Calculations" paragraph has been removed. The correct version was published on July 25, 2013.